Thermal Science and Engineering Progress 69 (2026) 104384

Contents lists available at ScienceDirect

Thermal Science and Engineering Progress

journal homepage: www.sciencedirect.com/journal/thermal-science-and-engineering-progress

Liquid nitrogen spray characterization in ambient and development of correlations for droplet diameter and velocity

Nishad Damle [a], Issam Mudawar [a,*], Jason Hartwig [b]

[a] Purdue University Boiling and Two-Phase Flow Laboratory (PU-BTPFL), School of Mechanical Engineering, Purdue University, 1500 Kepner Drive, Lafayette, IN 47905, USA

[b] Fluids and Cryogenics Branch, NASA Glenn Research Center, 21000 Brookpark Rd, Cleveland, OH 44135, USA

ARTICLE INFO

Keywords:
Cryogens
Sprays
Droplet diameter
Droplet velocity
Phase Doppler Particle Analyzer (PDPA)
Space applications

ABSTRACT

Sprays are among the most complex fluid systems to model and design. This study presents detailed measurements of droplet diameter and velocity for liquid nitrogen (LN_2) sprays discharged into ambient air. Using a high-resolution Phase Doppler Particle Analyzer (PDPA), both mean values and statistical distributions of droplet size and velocity were obtained. Five full-cone spray nozzles were tested across a range of injection pressures. PDPA data were used to develop new correlations for Sauter Mean Diameter (d_{32}), Arithmetic Mean Diameter (d_{10}), and Mean Droplet Velocity (u_f). Results show that increasing injection pressure leads to higher u_f but lower d_{32} values. Evaluation of existing d_{32} correlations—primarily developed for water sprays—revealed significant predictive errors when applied to LN_2 data. To address this, new dimensionless correlations were derived for d_{32}, d_{10}, and u_f, incorporating Reynolds and Weber numbers. These correlations demonstrated strong predictive performance when validated against the experimental data. The spray cone angle was found to be relatively insensitive to injection pressure but consistently smaller than the manufacturer's specified angle for water sprays. This reduction in cone angle is attributed not only to differences in thermophysical properties—such as viscosity, surface tension, and latent heat of vaporization—but also to ambient heat transfer causing evaporation at the spray's periphery, where droplet density is lowest. The newly developed LN_2 correlations provide valuable predictive tools essential for the design and optimization of cryogenic spray systems, particularly in future space applications.

1. Introduction

1.1. Cryogenic fluid Management for space Exploration

Cryogenic fluids—substances that remain in a liquid state at extremely low temperatures—are widely used across various industrial applications. As shown in Fig. 1, these ultra-low temperatures give cryogens unique thermophysical properties when compared to more conventional fluids such as water, refrigerants, and dielectric coolants. Notably, cryogenic liquids exhibit significantly lower viscosity, surface tension, and latent heat of vaporization than their near-room-temperature counterparts.

Cryogenic space propulsion systems are expected to play a critical role in extending human presence beyond Low Earth Orbit (LEO). One proposed approach to support such missions is the use of cryogenic fuel depots in *cis*-lunar space—Earth-orbiting propellant storage vessels designed to store cryogenic fuels and enable in-space refueling of vehicles.

As illustrated in Fig. 2, the transfer of cryogenic propellants from a storage tank to a receiving tank can be broken down into three key stages: (1) acquisition of the liquid from the storage tank, (2) chilldown of the transfer line hardware, and (3) chilldown and filling of the receiver tank. These stages involve several two-phase heat transfer and fluid flow processes, including pool boiling, flow boiling, and spray quenching. This study focuses specifically on the spray quenching process.

1.2. Predictive tools for cryogenic fluids

The effective design of cryogenic propellant transfer systems involving two-phase cryogenic flow relies heavily on accurate and reliable correlations at a fundamental level. Inaccurate or poorly validated models can lead to overly conservative designs, resulting in

* Corresponding author.
E-mail address: mudawar@ecn.purdue.edu (I. Mudawar).

https://doi.org/10.1016/j.tsep.2025.104384
Received 6 September 2025; Received in revised form 1 November 2025; Accepted 27 November 2025
Available online 4 December 2025

Nomenclature

d	droplet diameter (m)
d_0	orifice diameter (m)
d_{10}	Arithmetic Mean Diameter (m), Eq. (3)
d_{32}	Sauter Mean Diameter (m), Eq. (2)
d_{50}	Mass Median Diameter (m)
L	length of straight section in nozzle ending with orifice (m)
$\dot{m}$	mass flow rate of spray (kg/s)
N	number of data points
Oh	Ohnesorge number, $\mu_f/\sqrt{\rho_f \sigma d_0} = \sqrt{We_f}/Re_f$
Q	volumetric flow rate of spray (m^3/s)
P	injection pressure (Pa)
Re_f	Reynolds number of liquid at orifice, $(\rho_f U_f d_0)/\mu_f$
U_f	mean liquid velocity at orifice (m/s)
u_f	Mean Droplet Velocity (m/s)
We_f	Weber Number of liquid at orifice, $\left(\rho_f U_f^2 d_0\right)/\sigma$

Greek Symbols

μ	dynamic viscosity (kg/m.s)
ν	kinematic viscosity (m^2/s)
ρ	density (kg/m^3)
σ	surface tension (N/m)

Subscripts

0	orifice
a	ambient air
f	LN_2 liquid
g	LN_2 vapor
meas	measured
pred	predicted

Acronyms

AMD	Arithmetic Mean Diameter (d_{10})
CFD	Computational Fluid Dynamics
GFSSP	Generalized Fluid System Simulation Program
LEO	low Earth orbit
LN_2	Liquid nitrogen
MAE	Mean Absolute Error
MMD	Mass Mean Diameter (d_{50})
PDPA	Phase Doppler Particle Analyzer
PU-BTPFL	Purdue University Boiling and Two-Phase Flow Laboratory
PVC	Probe Volume Correction
SMD	Sauter Mean Diameter (d_{32})

increased safety margins, added system complexity, and higher costs.

Commonly used thermal/fluid simulation tools—such as the Generalized Fluid System Simulation Program (GFSSP) and SINDA/FLUINT [1]—support the design of these systems. These are lumped-parameter codes that rely on empirical correlations to model single- and two-phase flow, pressure drops, and heat transfer. However, numerous studies have shown that the correlations currently implemented in these tools often do not align well with experimental data for cryogenic two-phase flow and heat transfer [2].

Accurately predicting two-phase flow and heat transfer has long been a central focus of research at the Purdue University Boiling and Two-Phase Flow Laboratory (PU-BTPFL). This effort spans a wide range of working fluids and encompasses nearly every conceivable two-phase flow regime: capillary flow [3], pool boiling [4], falling-film flow [5,6], channel flow [7,8], micro/mini-channel flow [9], jet impingement [10], and spray cooling [11], as well as hybrid approaches that integrate the benefits of multiple schemes [12].

The present study continues PU-BTPFL's ongoing research, with a particular emphasis on the unique transport phenomena associated with cryogenic sprays.

1.3. Two-Phase hydrodynamics of sprays

Sprays play a vital role across a wide range of industries, including fuel injection, pharmaceuticals, crop fertilization, painting, and metal alloy quenching—not to mention aerospace applications, which are the focus of the present study. In general, sprays rely on the momentum of liquid expelled from a nozzle to break up into fine droplets. This atomization significantly increases the liquid's surface area-to-volume ratio, enhancing its effectiveness in cooling hot surfaces. Additionally, sprays promote a more uniform spatial distribution of heat removal.

Despite their advantages, the practical implementation of sprays presents numerous challenges. As noted in [13], these challenges stem from the complex and highly parameter-dependent nature of spray flow and heat transfer behavior. Key variables include flow conditions (nozzle type, pressure drop, flow rate), system geometry (orifice diameter, cone angle, orifice-to-surface distance, surface size), and spray hydrodynamics (mean droplet diameter, droplet velocity, volumetric flux, and their spatial distributions). This intricate interdependence makes it particularly difficult to accurately predict the heat transfer characteristics of spray systems.

A comprehensive review of spray hydrodynamics and heat transfer is provided in [14,15], covering dominant physical mechanisms, key hydrodynamic parameters influencing spray behavior, correlations for mean droplet diameter and velocity, as well as heat transfer correlations across different regimes of the boiling curve and their transition points. However, because much of the reviewed literature focuses on the quenching of metal alloy parts, the majority of the correlations are based on water as the working fluid. Studies involving alternative coolants—particularly cryogens—remain relatively limited.

Using FC-72 as the working fluid, Estes and Mudawar [16] conducted detailed measurements of spray characteristics using a Phase Doppler Particle Analyzer (PDPA). They measured the Sauter Mean Diameter (SMD), d_{32}, and volumetric flux for three UniJet nozzles (Spraying Systems Co.) with orifice diameters ranging from $d_0 = 0.762$ to 1.700 mm. By combining these FC-72 measurements with data from earlier studies on water sprays [17], they developed correlations for d_{32} that proved highly effective in predicting critical heat flux (CHF) across three different fluids: water, FC-72, and FC-87.

Much of the published PDPA droplet characterization research focuses on fluids at much higher temperatures and with thermophysical properties that differ significantly from those of cryogens. However, there are a few notable exceptions. One such study is by Liu et al. [18], who investigated the effects of injection pressure on droplet size distribution and spray cone angle for liquid nitrogen (LN_2). Another is the work by Xue et al. [19], who measured the hydrodynamic characteristics of LN_2 sprays injected into ambient air using two different fog nozzles.

Recent cryogenic spray experiments employing PDPA or PDI diagnostics have begun to elucidate the spatial evolution of droplet size and velocity fields in liquid oxygen (LOX) and liquid nitrogen (LN_2) under flashing or superheated conditions. Rees et al. [20] used PDPA/PDA measurements in flash-boiling LN_2 jets and showed that superheated injection induces highly violent primary breakup, large spray cone angles, significant axial reduction of Sauter mean diameter, and—in certain cases—two distinct droplet populations in the near field associated with ligament shedding and secondary breakup. Fdida et al. [21] applied PDI to LOX injection in a coaxial configuration and characterized near-nozzle droplet diameter and velocity distributions,

revealing that large liquid structures persist within the jet core while smaller droplets are convected radially outward. Classic liquid-nitrogen studies by Ingebo [22] further demonstrated that evaporation and flashing strongly influence measured droplet size and must be considered integral components of the breakup process rather than as downstream evaporation phenomena. Collectively, these studies indicate that cryogenic sprays undergo rapid disintegration and exhibit extremely dispersed droplet fields near the nozzle, which subsequently collapse into a narrower size distribution farther downstream. Nonetheless, spatially resolved, high-resolution LN_2 data for single-orifice injectors remain scarce.

At ambient conditions, PDPA and PDI diagnostics have also been extensively applied to water, air-blast, and fuel sprays, establishing benchmark trends for the coupled evolution of droplet size and velocity with injector geometry and operating pressure. Wang et al. [23] characterized pressure-swirl water nozzles and identified distinct axial development zones in which mean droplet size and local axial velocity evolve in tandem, with the droplet size distribution progressively narrowing downstream. Soni et al. [24] investigated annular-swirl air-blast atomization and demonstrated that increasing aerodynamic shear—by raising the air-to-liquid momentum ratio—shortens the breakup length, reduces the Sauter mean diameter, and produces broader radial velocity profiles populated by smaller, higher-speed droplets. Patil et al. [25] further showed that injector geometry and imposed swirl directly govern axial velocity decay and droplet size reduction in twin-jet air-blast injectors. Collectively, these ambient-pressure studies establish a consistent trend: smaller nozzle orifices and stronger aerodynamic forcing yield larger apparent cone angles, higher initial droplet velocities, and

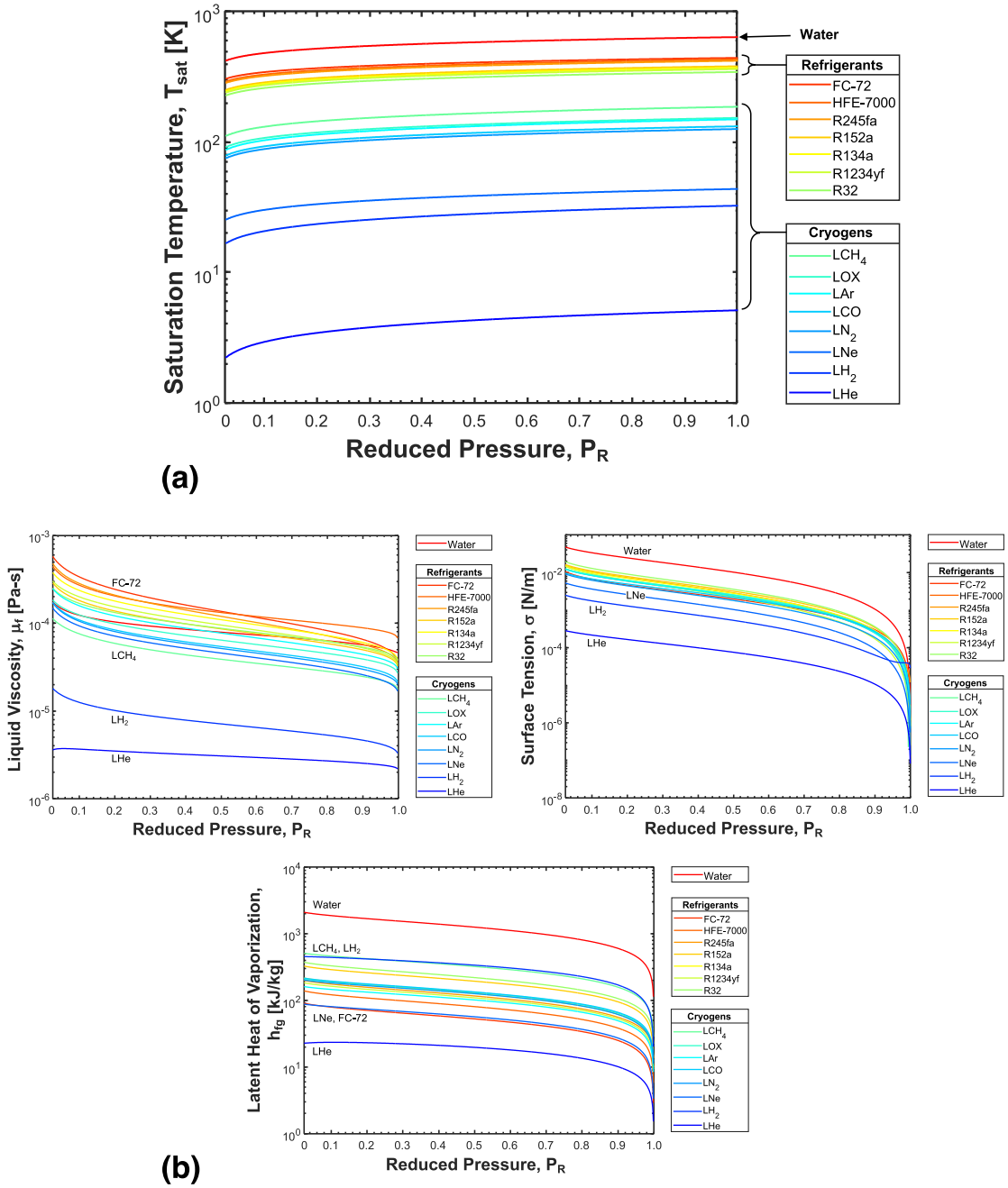

Fig. 1. (a) Classification of coolants into water, refrigerants, and cryogens based on variation of saturation temperature with reduced pressure. (b) Low liquid viscosity, surface tension, and latent heat of vaporization of cryogens compared to other fluids.

greater overall droplet dispersal.

Li et al. [26] examined the flash-boiling breakup process in gasoline-type fuel injection systems and demonstrated that superheating beyond the threshold required at the nozzle exit produces explosive atomization, extensive plume spreading, drastic reductions in mean droplet size, and, under the most extreme conditions, plume coalescence. Akram et al. [27] compared several superheated fuel sprays and found that elevated superheat levels consistently decrease the Sauter mean diameter and shorten the axial distance required for complete fuel dispersion. In their combined experimental–computational investigation, Payri et al. [28] underscored the importance of accurate near-nozzle measurements of droplet size and velocity for developing reliable numerical models of flash-boiling sprays in gasoline direct injection systems.

Spray–spray impingement studies using binarized plume imaging have shown that when interacting plumes exceed a critical overlap, local fuel–air mixing becomes dominated by the impingement process itself rather than by the dynamics of individual jets [29]. A companion comparative investigation employed the same binarization and normalization methodology to analyze both single-hole and multi-hole injectors, thereby establishing a unified basis for comparing penetration, cone angle, and plume interaction characteristics across different injector geometries under engine-relevant pressures [30].".

1.4. Objectives of present study

As noted above, spray hydrodynamics—such as droplet breakup at the orifice due to hydrodynamic instabilities, spray angle, droplet trajectory, droplet size distribution, and velocity distribution—are highly dependent on the nozzle type, working fluid, and operating conditions. Predictive methods for spray behavior are typically developed for specific applications and are therefore fluid-specific.

Given the unique characteristics of cryogenic fluids—including their extremely low saturation temperatures and distinct thermophysical properties (notably low liquid viscosity, surface tension, and latent heat of vaporization)—the accuracy of conventional predictive tools is significantly compromised when applied to cryogenic sprays. This challenge is compounded by the limited number of published studies that focus specifically on the characterization of cryogenic spray behavior.

A long-term objective of this study is to address the gaps in predictive capabilities for cryogenic sprays, particularly in the context of space applications. The current goal is to conduct extensive PDPA characterization of liquid nitrogen (LN_2) sprays under terrestrial gravity conditions, covering a wide range of variables including nozzle type, orifice size, injection pressure, injection temperature, subcooling, and flow rate. Measurements are taken at multiple axial and lateral locations within the spray to develop new, high-accuracy correlations for droplet diameter and droplet velocity. Spray angle is also measured under the same operating conditions to provide a comprehensive understanding of spray behavior.

This foundational work sets the stage for future cryogenic spray experiments planned aboard parabolic flight aircraft. These upcoming studies will investigate the additional effects of reduced gravity environments—such as microgravity, Lunar gravity, and Martian gravity—on spray hydrodynamics and heat transfer.

The primary objectives of this study are to:

(a) Measure spray angle for multiple nozzles across a selected matrix of operating conditions.
(b) Measure Sauter Mean Diameter (SMD) at various locations along the spray axis and laterally across the spray.
(c) Measure Mean Droplet Velocity at various locations along the spray axis and laterally across the spray.
(d) Develop new empirical correlations for SMD and droplet velocity specific to liquid nitrogen (LN_2).

2. Experimental methods

The experimental setup for this study consists of two main components: the PDPA system and the spray delivery system.

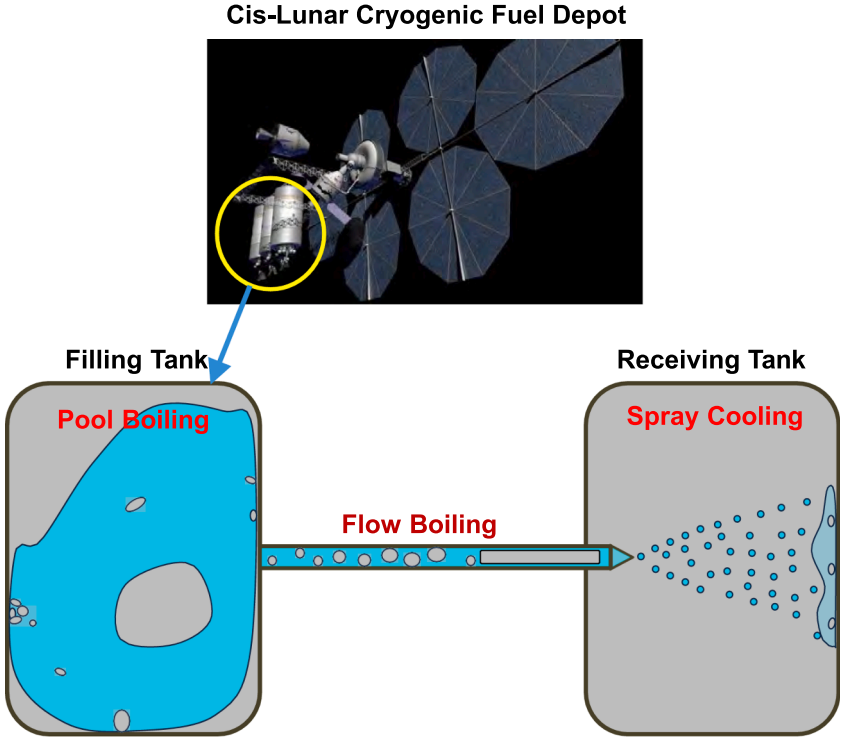

Fig. 2. Schematic representation of *cis*-Lunar cryogenic fuel transfer from fuel depot to space vehicle, and relevant two-phase transport processes.

2.1. Spray characterization using phase Doppler Particle Analyzer (PDPA)

2.1.1. Principle of Operation and Layout of PDPA system

The Phase Doppler Particle Analyzer (PDPA) is a laser-based diagnostic instrument that utilizes principles of light scattering and phase shift measurement to deliver highly accurate, non-intrusive assessments of droplet size, velocity, and other characteristics in sprays and multiphase flows. Its optical measurement technique allows researchers to study complex flow dynamics without physically disturbing the system, making it especially valuable in applications where system integrity is critical.

In the present study, the PDPA was chosen specifically for its precision and reliability in spray diagnostics. A key goal of this work is to address the current lack of detailed information on cryogenic sprays—particularly liquid nitrogen—by using PDPA measurements to assess the applicability and limitations of existing spray correlations developed for room-temperature fluids when applied to cryogenic conditions.

The PDPA system analyzes these fringe patterns to extract both droplet size and velocity information. As light interacts with the droplet, phase differences arise between the signals received by the multiple detectors. These phase differences are linearly proportional to the droplet's diameter, allowing for precise size measurements. Larger droplets produce broader fringe spacing and smaller phase shifts, while smaller droplets generate narrower fringes and greater phase shift differences. This linear relationship enables the PDPA to accurately measure a wide range of droplet sizes.

Figs. 3 and 4 provide a basic overview of the PDPA measurement technique and the specific PDA system components used in the present study, respectively.

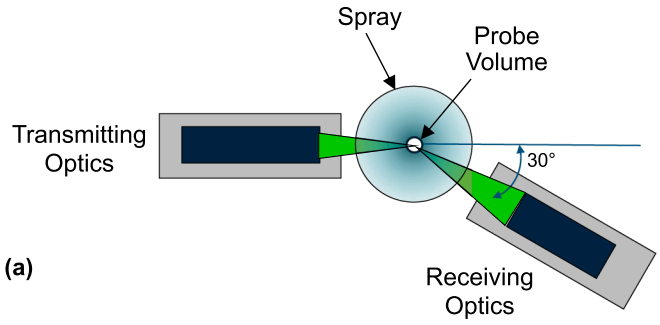

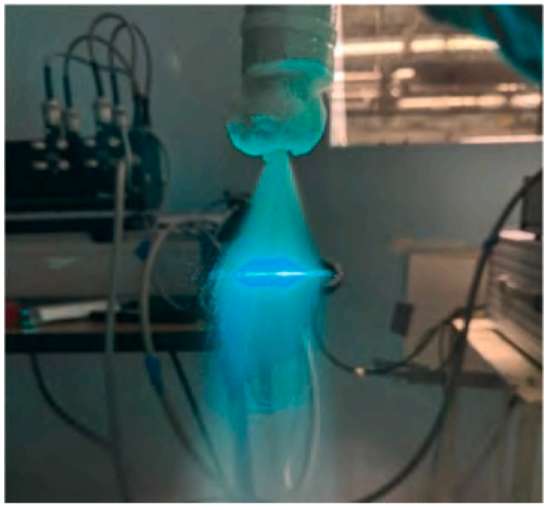

Fig. 3. (a) PDPA technique. (b) Image of probe volume capture in LN_2 spray.

As shown in Fig. 4, our PDPA system consists of several key components, each playing a vital role in the measurement process. A Dantech 300-mW argon-neon laser, along with transmitting optics—including a beam splitter, frequency shifter, and focusing lens—generates coherent laser beams in green (514.5 nm) and blue (488 nm) wavelengths. These beams intersect to form a well-defined probe (measurement) volume, which represents the region where droplets scatter light. The small size of this probe volume ensures that individual droplets can be analyzed without interference from neighboring droplets.

The scattered light is collected by the system's receiving optics, which are positioned at a specific refraction angle—typically 30° for water, but optimized here for LN_2. A TSI receiving lens focuses the scattered light onto a set of three photodetectors arranged to detect phase differences and intensity patterns essential for determining droplet size and velocity. The system also includes a TSI signal processing module that converts the raw optical signals into usable droplet diameter and velocity data. With high temporal resolution, the TSI system allows the PDPA to capture transient events within rapidly evolving spray environments—making it particularly well-suited for the dynamic behavior of cryogenic sprays.

A dedicated computer processes the raw data to generate droplet diameter and velocity distributions, as well as mean values for each. The use of multiple independent detections for each droplet enhances the reliability and accuracy of the measurements, even in challenging conditions such as dense sprays where signal quality may be compromised.

In this study, the optimum refraction angle of 28° for LN_2 was accurately determined by adjusting the position of the receiving lens relative to the probe volume to achieve the strongest signal and the highest data acquisition rate.

2.1.2. Validation techniques and error Minimization

The accuracy of PDPA measurements is maintained through a series of validation techniques aimed at improving data reliability and minimizing error. One of the primary methods employed is intensity validation, which distinguishes valid signals from noise by analyzing the intensity patterns of scattered light. Techniques such as the 1/3 Dmax Method are used to set threshold levels for acceptable signal intensity, ensuring that only high-quality data are processed. This validation is especially critical in environments prone to multiple scattering or high background noise, where signal contamination could otherwise compromise measurement accuracy.

Another important validation method is Probe Volume Correction (PVC), which addresses measurement biases resulting from non-uniform intensity distributions within the probe volume. Smaller droplets, for example, may scatter light less efficiently or unevenly, potentially leading to underestimation of their size. PVC compensates for these biases by normalizing the intensity distribution across the probe volume, ensuring that droplets of all sizes—both small and large—are accurately represented in the measured data.

Phase validation provides an additional layer of quality control by verifying the consistency of phase differences used to calculate droplet diameter. This technique is especially valuable in dense sprays or when droplets pass off-center through the probe volume, conditions that can introduce measurement errors. By comparing phase signals from multiple detectors, the system can identify inconsistencies indicative of trajectory deviations or mixed-mode scattering. Erroneous data can then be excluded, improving the overall reliability and accuracy of the measurements.

Together, these validation techniques ensure that the PDPA provides high-quality, reliable measurements across a wide range of operating conditions. Overall, the measurement uncertainty in the present study is estimated to be less than 10 % for droplet diameter and less than 15 % for droplet velocity.

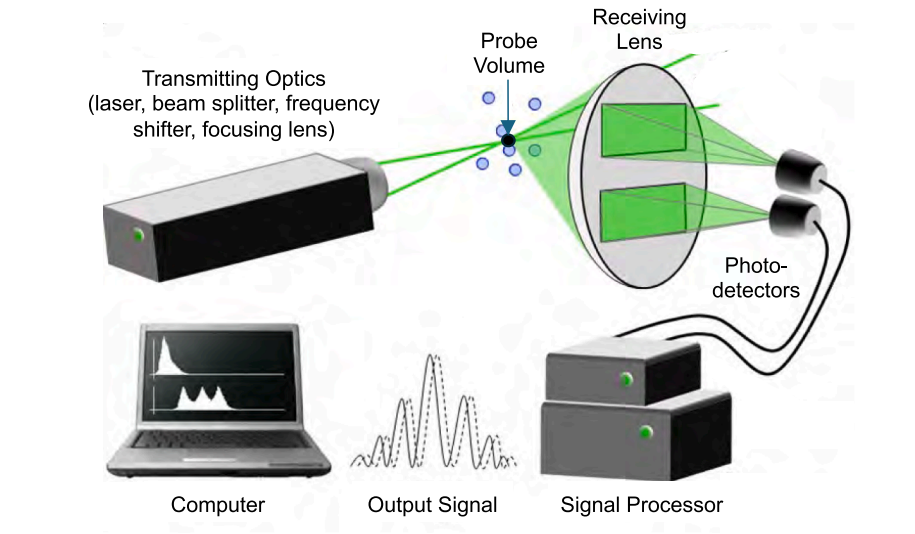

Fig. 4. (a) Components of PDPA system. (b) Photo of PDPA system used in the present study.

2.2. Other optical method for capturing Spray's cone angle

Two different video systems were used to capture side-view imagery of the spray. The first system was a Photron FASTCAM-Ultima APX high-speed video camera, capable of capturing full megapixel resolution at 3,000 frames per second (fps), 512 × 512 pixels at 10,000 fps, and lower resolutions at frame rates up to 250,000 fps. However, in practice, the effective resolution was constrained by the strength of the backlighting. As a result, a frame rate of 6,000 fps was selected for this study to achieve an optimal balance between resolution and illumination for spray visualization.

The second system was a Sony RX10 IV digital camera paired with a TTL flash, used for short-duration video capture at frame rates up to 1,000 fps. This setup provided additional flexibility for capturing spray dynamics under varying lighting.

Once the images were captured, the spray angle analysis was performed using ImageJ software. Prior to the measurement, binarization processing was applied to the spray images to clearly distinguish the spray boundary from the background. The threshold value was determined using ImageJ's auto-threshold function, specifically employing the Triangle method, which provided consistent detection of the spray boundaries across all test conditions. This approach ensured objective and reproducible extraction of the spray cone geometry for accurate angle determination.

Fig. 5 shows spray images captured using both video systems for Nozzles D1 and D4 (details provided later) at an injection pressure of 413.69 kPa (60 psi). Despite the high frame rate capability of the FASTCAM system, it was not sufficient to capture the fastest-moving droplets within the spray. However, droplet velocity measurements were independently obtained using the PDPA system. As a result, the two camera systems were used exclusively for capturing the spray cone angle, rather than droplet-level motion.

2.3. Spray delivery system

The LN_2 fluid delivery system was designed to generate a stable spray that consistently intercepts the PDPA probe volume. As illustrated in Fig. 6, nitrogen gas from a pressurized cylinder is used to drive liquid

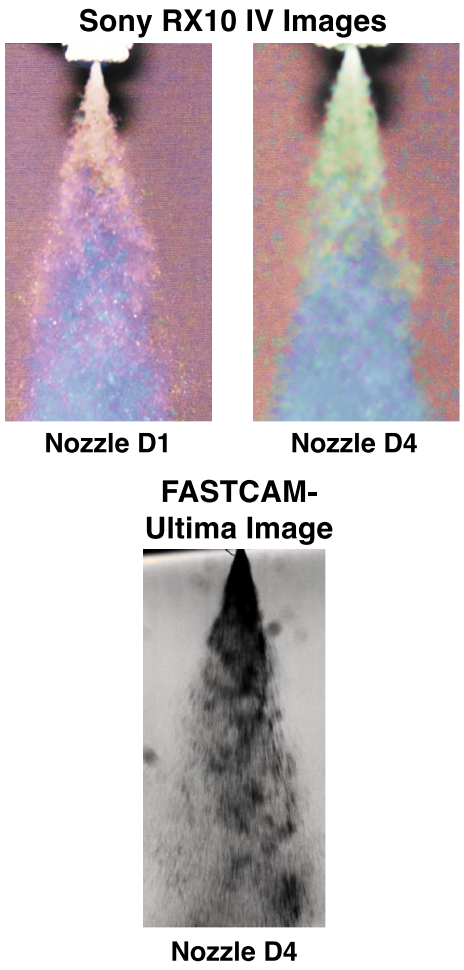

Fig. 5. Spray images captured using two camera systems.

nitrogen (LN_2) from a 160 L dewar through the downstream components of the system. Upon exiting the dewar, the LN_2's temperature, pressure, and volumetric flow rate are measured before the fluid enters a pre-cooler, which sets the desired degree of subcooling.

The pre-cooler consists of a multi-coil copper tube immersed in an LN_2 bath at ambient pressure. The coiled configuration increases the surface area for heat exchange, allowing the flowing LN_2 to cool below its saturation temperature at the system pressure. Subcooling is achieved because the LN_2 in the delivery system is at a higher saturation pressure—and thus temperature—than the ambient pressure LN_2 bath. To maintain the bath level and offset evaporative losses during testing, LN_2 is continuously supplied from a separate dewar.

Downstream of the pre-cooler, the LN_2 temperature and pressure are measured again to precisely determine the fluid state at the nozzle inlet and to accurately convert volumetric flow rate into mass flow rate. The spray is formed at ambient pressure by the nozzle. To accelerate initial system chill-down, a bleed line positioned downstream of the nozzle is used to purge warm fluid; this line is closed off once the system is sufficiently chilled, to sustain a stable spray cone, and before PDPA data acquisition begins. The liquid is discharged through the orifice which results in enough flow inertia to prevent icing at the orifice or inside the nozzle. Consequently, no evidence of icing was observed in the present experiments and the nozzle outlet geometry remained unaffected across all the test conditions.

All temperature measurements in the system were made using OMEGA Type-E grounded thermocouples, which offer an accuracy of ± 1.0 °C. Pressure measurements were obtained using OMEGA PX409 pressure transducers with a rated accuracy of ± 0.08 %. Because these transducers are not rated for cryogenic temperatures, each was installed away from the main LN_2 flow using a 3.175 mm (1/8 in), 60 cm long coiled stainless-steel tube. This configuration allows the LN_2 to vaporize and warm up sufficiently before reaching the transducer, preventing cryogenic damage and ensuring accurate pressure readings.

Volumetric flow rate was measured using a Flow Technology FT8-8 turbine flow meter, which provides a measurement accuracy of ± 0.1 %.

To achieve comprehensive mapping of droplet diameter and velocity throughout the spray, PDPA measurements were taken at selected locations both along the spray axis and laterally across it, perpendicular to the axis. Vertical alignment of the spray nozzle with the desired measurement height was accomplished by adjusting the length of the vertical tubing leading to the nozzle. Likewise, lateral positioning was achieved by varying the length of the horizontal tubing feeding into the nozzle axis.

Fine positioning of the PDPA probe volume within the spray was accomplished by mounting both the transmitting and receiving optics in tandem on manual translation stages. This setup allowed for precise alignment of the measurement volume with the targeted regions of the spray.

The spray nozzles characterized in this study are stainless-steel full-cone UniJet series D and TG nozzles manufactured by Spraying Systems Co. Each D-series nozzle consists of three main components: a strainer (to remove particles from the flow), a liquid swirling core, and an orifice plate disc that promotes liquid breakup into a full cone spray pattern. The TG-series nozzles feature a similar internal structure but with a consolidated, one-piece construction.

Fig. 7 provides detailed illustrations of the internal construction and liquid flow paths for both nozzle types.

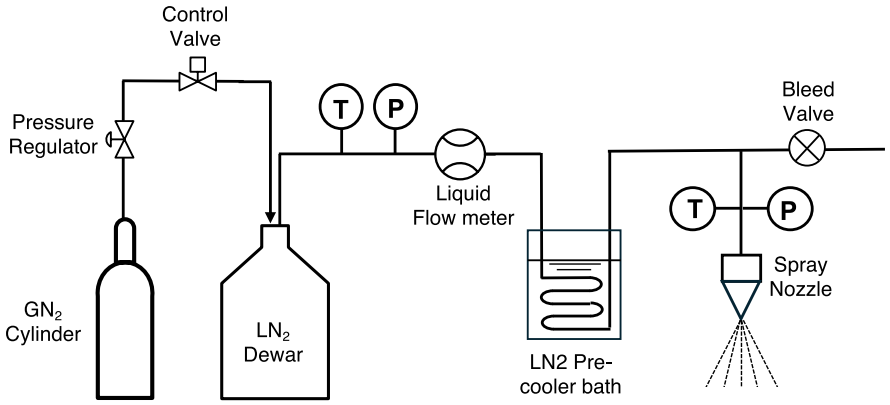

Fig. 6. Schematic diagram of spray delivery system.

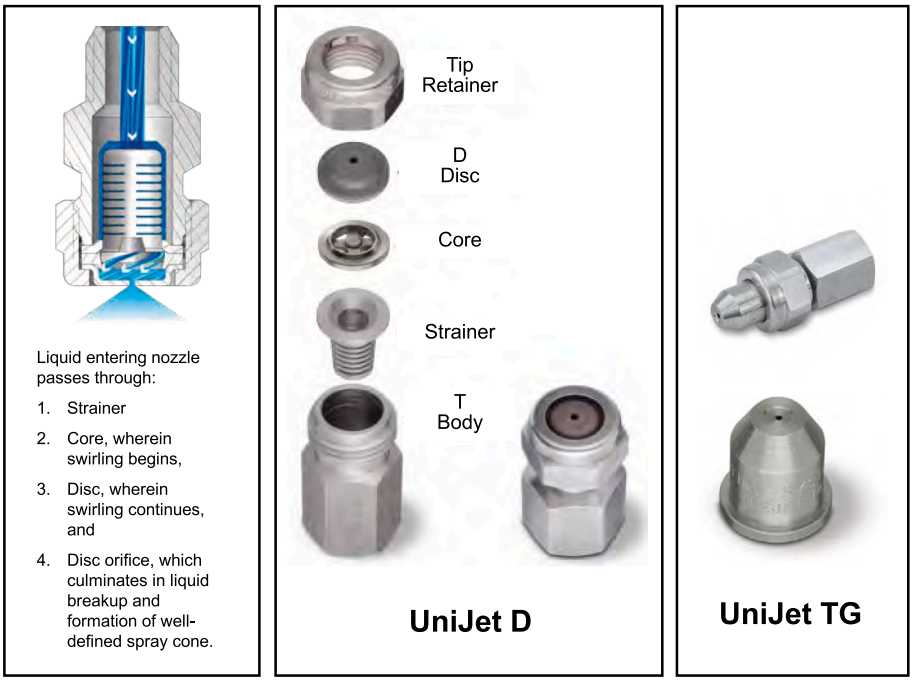

Nozzle	Orifice Diameter
D4	0.063 in (1.600 mm)
D3	0.047 in (1.194 mm)
D1	0.031 in (0.787 mm)
TG2	0.047 in (1.194 mm)
TG 0.5	0.024 in (0.610 mm)

Fig. 7. Construction of the Spraying System's UniJet nozzles characterized in the present study.

2.4. Experimental operating conditions and PDPA probe volume locations

Table 1 presents the orifice diameter for each nozzle along with the corresponding experimental operating conditions. In this study, subcooling upstream of the nozzle is defined as the difference between the saturation temperature corresponding to the injection pressure and the actual injection temperature.

Experiments were conducted over an injection pressure range of 344.74 to 620.52 kPa, controlled by throttling the nitrogen gas flow into the dewar. All tests were performed with the spray discharging into ambient atmospheric pressure air and all measurements were taken after the spray became fully developed to avoid any transient chill down data recording. For each nozzle, the injection pressure largely dictated the resulting flow rate, although this relationship was also influenced—albeit to a lesser extent—by the degree of subcooling upstream of the nozzle. Subcooling levels varied from 8 to 15 °C, depending on the cooling rate in the pre-cooler, which was adjusted as needed to ensure a fully developed spray.

The PDPA system was used to collect detailed droplet diameter and velocity distributions. As shown in Fig. 8, data were acquired at four axial distances from the nozzle orifice: 38.1, 76.2, 114.3, and 152.4 mm. To evaluate the symmetry of the spray cone, two to four additional lateral measurements were conducted at each axial position.

The data rates for presented data were between 600 Hz and 3000 Hz depending on the location within the spray and the operating conditions. Intensity validation and phase validation were performed as per the recommendation of the manufacturer of the PDPA system. For all the presented data, the burst threshold efficiency is over 55 %. During the measurements, the Phase AB and Phase AC were matched with certainty usually within 5–10 %, although the inbuilt thresholds within the PDPA processing systems account for this.

3. Experimental results and discussion

3.1. Diameter and velocity distributions

Figs. 9–13 present the complete PDPA measurement results for nozzles D1, D3, D4, TG0.5, and TG2, respectively. Each figure displays the axial measurement location (i.e., the distance from the nozzle orifice to the PDPA probe volume) and the injection pressures tested, as indicated at the top of the figure.

On the left side of each figure are plots showing the spatial variation of Sauter Mean Diameter (SMD) and mean droplet velocity, both along the spray axis and laterally outward from the axis at each axial location. As shown earlier in Fig. 8, the lateral extent of these SMD and velocity profiles reflects the spray cone angle for each case.

Table 1
Orifice diameters and detailed operating conditions for the tested spray nozzles.

Injection Pressure [kPa]	Injection Temperature [°C]	Subcooling [°C]	Mass Flow Rate [kg/s]
Nozzle D1 (0.787 mm)			
413.69 (60 psi)	−191.5 to −190	9 to 10	0.0069
482.63 (70 psi)	−181 to −180	9 to 10	0.0078
551.58 (80 psi)	−193.6 to −192.6	9 to 10.5	0.0097
Nozzle D3 (1.194 mm)			
344.74 (50 psi)	−193.6 to −192.6	9 to 10	0.0154
413.69 (60 psi)	−191.5 to −190.5	9 to 10	0.0173
482.63 (70 psi)	−190.5 to −189.5	9 to 10	0.0187
551.58 (80 psi)	−188.4 to −187.4	9 to 10	0.0198
620.52 (90 psi)	−186.3 to −185.3	9 to 10	0.0203
Nozzle D4 (1.600 mm)			
344.74 (50 psi)	−193.7 to −191.7	9 to 10	0.0216
413.69 (60 psi)	−189.5 to −188.0	8 to 9	0.0296
482.63 (70 psi)	−189.4 to −188.8	9 to 10	0.0391
551.58 (80 psi)	−186.4 to −185.4	8 to 10	0.0410
620.53 (90 psi)	−186.5 to −185.5	9 to 10	0.0443
Nozzle TG0.5 (0.610 mm)			
344.74 (50 psi)	−192.6 to −189.0	5 to 9	0.0039
413.69 (60 psi)	−191.5 to −190.5	9 to 10	0.0044
482.63 (70 psi)	−192.5 to −188.5	9 to 13	0.0049
551.58 (80 psi)	−188.8 to −186.8	9 to 11	0.0058
620.53 (90 psi)	−189.3 to −186.3	10 to 13	0.0068
Nozzle TG2 (1.194 mm)			
344.74 (50 psi)	−193.6 to −192.6	9 to 10	0.0169
413.69 (60 psi)	−191.5 to −190.5	9 to 10	0.0182
482.63 (70 psi)	−191.5 to −189.2	10 to 12	0.0204
551.58 (80 psi)	−189.8 to −186.8	9 to 12	0.0224
620.53 (90 psi)	−191.3 to −186.3	10 to 15	0.0255

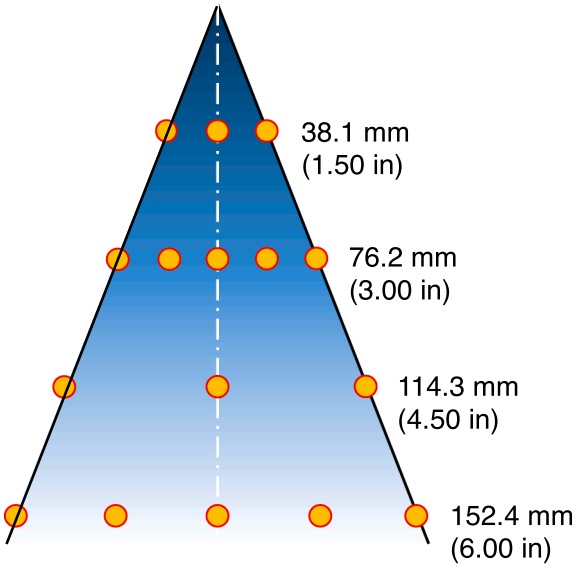

Fig. 8. Locations of PDPA measurements within the spray.

To the right of the spray data plots are representative distribution histograms for droplet diameter and droplet velocity, illustrating the statistical spread and behavior of the measured data.

Several important inferences can be drawn form the PDPA data plots:

Overall Effects of Injection Pressure on SMD and Mean Droplet Velocity: The data plots for nozzle D1 at axial distances of 38.1 mm and 76.2 mm (Fig. 9a) demonstrate a clear and systematic influence of injection pressure on both Sauter Mean Diameter (SMD) and mean droplet velocity along the spray axis. In general, higher injection pressures result in decreased SMD—indicative of finer atomization—and increased droplet velocities. Similar trends are observed for D1 at greater axial distances (114.3 mm and 152.4 mm) in Fig. 9b. Consistent behavior is also evident in Figs. 10–13 for nozzles D3, D4, TG0.5, and TG2, respectively, though some anomalies are present. A notable example occurs in the SMD data for nozzle D4 at 38.1 mm, which deviates from the expected trend. This discrepancy may be attributed to one or more of the following factors: (i) PDPA measurement uncertainty, (ii) variations in subcooling affecting fluid properties and breakup dynamics, (iii) incomplete droplet breakup at this near-nozzle location, and (iv) axial vaporization of LN_2 droplets upon injection into ambient air. Aside from such outliers, the overall trends remain consistent across nozzle types and operating conditions: increased injection pressure promotes finer droplet breakup and higher droplet velocities.

Effects of Axial Location: The data plots for nozzle D1 (Fig. 9a) show an increase in SMD between 38.1 mm and 76.2 mm, while mean droplet velocity remains relatively constant between these two axial positions. A similar velocity trend is observed between 114.3 mm and 152.4 mm (Fig. 9b), although in this case, the SMD trend reverses—decreasing with increasing distance. For nozzle D3, Fig. 10a shows a slight increase in SMD between 38.1 mm and 76.2 mm, accompanied by a decrease in mean velocity. These trends are also evident at farther axial locations (114.3 mm and 152.4 mm) in Fig. 10b. For nozzle D4, both SMD and velocity decrease between 38.1 mm and 76.2 mm, while between 114.3 mm and 152.4 mm (Fig. 11b), SMD remains fairly constant and velocity increases modestly. In the case of TG0.5, the axial variations in both SMD and velocity are more attenuated than in D1, D3, or D4—both between 38.1 mm and 76.2 mm (Fig. 12a) and between 114.3 mm and 152.4 mm (Fig. 12b). For nozzle TG2, SMD remains within a narrow range while mean velocity increases between 38.1 mm and 76.2 mm (Fig. 13a). Between 114.3 mm and 152.4 mm (Fig. 13b), both SMD and velocity exhibit minimal variation. Overall, axial location shows the most inconsistency in trends of SMD and velocity. Unlike the clear pressure-dependent trends observed earlier, axial evolution of spray characteristics appears less systematic. As previously discussed in the context of injection pressure anomalies, these inconsistencies may be attributed to several factors: (i) PDPA measurement uncertainties, (ii) variations in subcooling that alter fluid properties and breakup dynamics, (iii) incomplete droplet breakup at near-nozzle locations (e.g., 38.1 mm), and (iv) axial vaporization of LN_2 droplets upon exposure to ambient air.

Effects of Lateral Spread: UniJet nozzles are designed to produce axisymmetric full-cone sprays. However, due to the previously discussed anomalies and inconsistencies, deviations from perfect symmetry are observed in several cases. Notable examples include nozzle D1 at 76.2 mm (Fig. 9a), D3 at both 38.1 mm and 76.2 mm (Fig. 10a), and TG2 at 38.1 mm (Fig. 13a). In these cases, lateral profiles of SMD and/or mean velocity appear skewed or asymmetric, likely due to localized irregularities in droplet breakup, PDPA measurement variation, or unsteady spray dynamics near the nozzle. In contrast, several cases exhibit clear symmetry. For example, nozzle D4 at 114.3 mm and 152.4 mm (Fig. 11b) shows laterally symmetric SMD and velocity profiles. I n these symmetric cases, SMD profiles tend to be concave upward while velocity profiles are concave downward. This behavior reflects the expected spray structure: droplets near the centerline, most directly influenced by the injection pressure and core spray momentum, are typically smaller—due to more complete breakup—and faster. In contrast, droplets farther from the axis, influenced by frictional losses along the periphery of the orifice, are subject to reduced local pressure. This results in larger, slower droplets due to weaker atomization and lower momentum.

Effects of Orifice Diameter: Nozzles D1, D3, and D4 share the same internal construction but differ in orifice diameter, with values of 0.787 mm, 1.194 mm, and 1.600 mm, respectively. However, comparisons of SMD and mean droplet velocity at identical axial

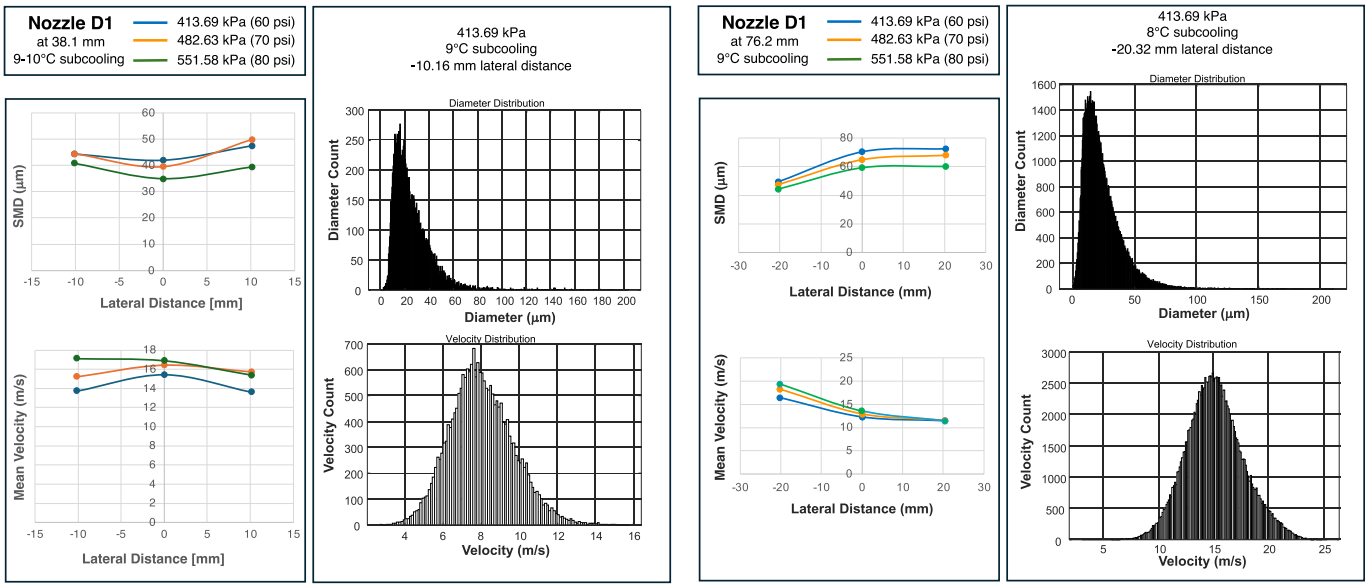

Fig. 9a. PDPA measurements for nozzle D1 at axial distances of 38.1 and 76.2 mm.

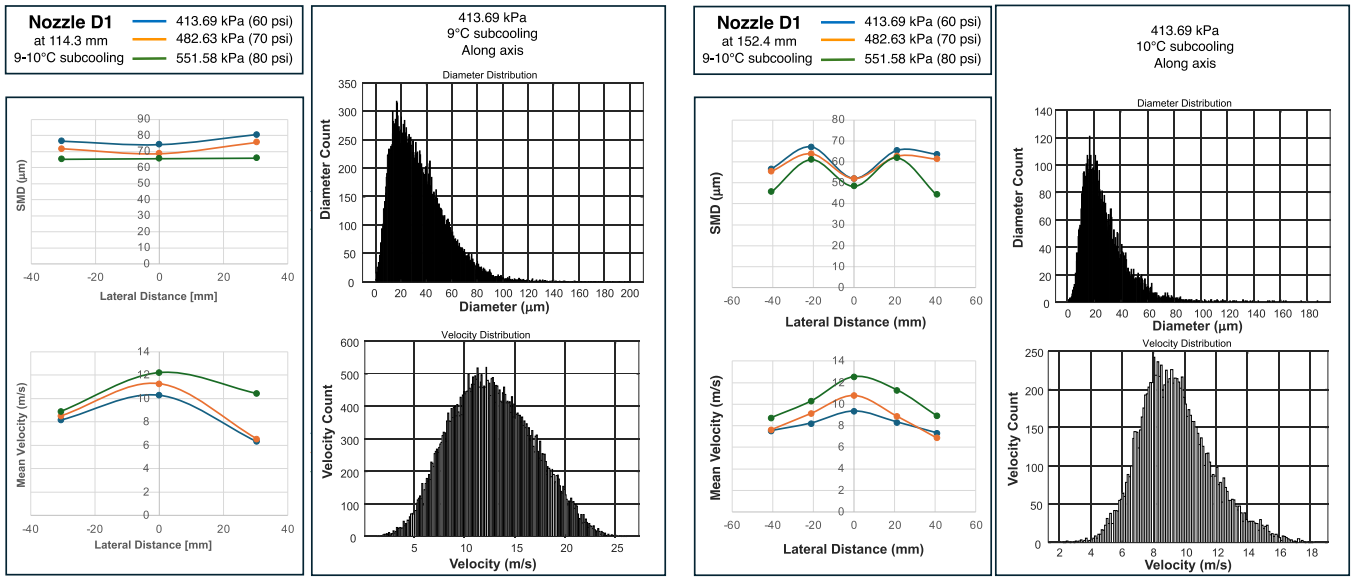

Fig. 9b. PDPA measurements for nozzle D1 at axial distances of 114.3 and 152.58 mm.

locations across these three nozzles do not reveal consistent or systematic trends. This suggests that, for a given injection pressure, increasing the orifice diameter primarily affects the volumetric flow rate (as shown in Table 1) rather than directly influencing droplet size or velocity. A similar inference can be made for nozzles TG0.5 and TG2, which also have similar internal construction but differing orifice diameters of 0.610 mm and 1.194 mm, respectively. Again, variations in SMD and velocity are not consistently correlated with orifice size, reinforcing the conclusion that orifice diameter's dominant influence is on flow rate rather than on spray breakup characteristics under the tested conditions.

Statistical Distributions: Figs. 9–13 reveal consistent statistical patterns across all tested nozzles. The droplet velocity distributions generally follow a symmetrical Gaussian (normal) profile, indicating uniformity in droplet acceleration and momentum transfer. In contrast, the droplet diameter distributions tend to be skewed toward smaller values, suggesting a higher frequency of smaller droplets within the spray. This skewness is typical of atomization processes, where a range of breakup mechanisms leads to a predominance of fine droplets alongside fewer large ones.

Overall, the PDPA results exhibit mostly consistent trends with respect to injection pressure and axial distance from the nozzle orifice. However, the influence of other parameters—such as lateral position and orifice diameter—shows less consistency. This variability reflects the inherent complexity of spray dynamics, a challenge well-documented in prior studies [13–15]. Such complexities underscore the need for high-fidelity measurements and fluid-specific correlations, particularly for cryogenic spray systems.

3.2. Diameter and velocity correlations

One primary aim of this study is to develop new empirical correlations for droplet diameter and velocity using the extensive PDPA data

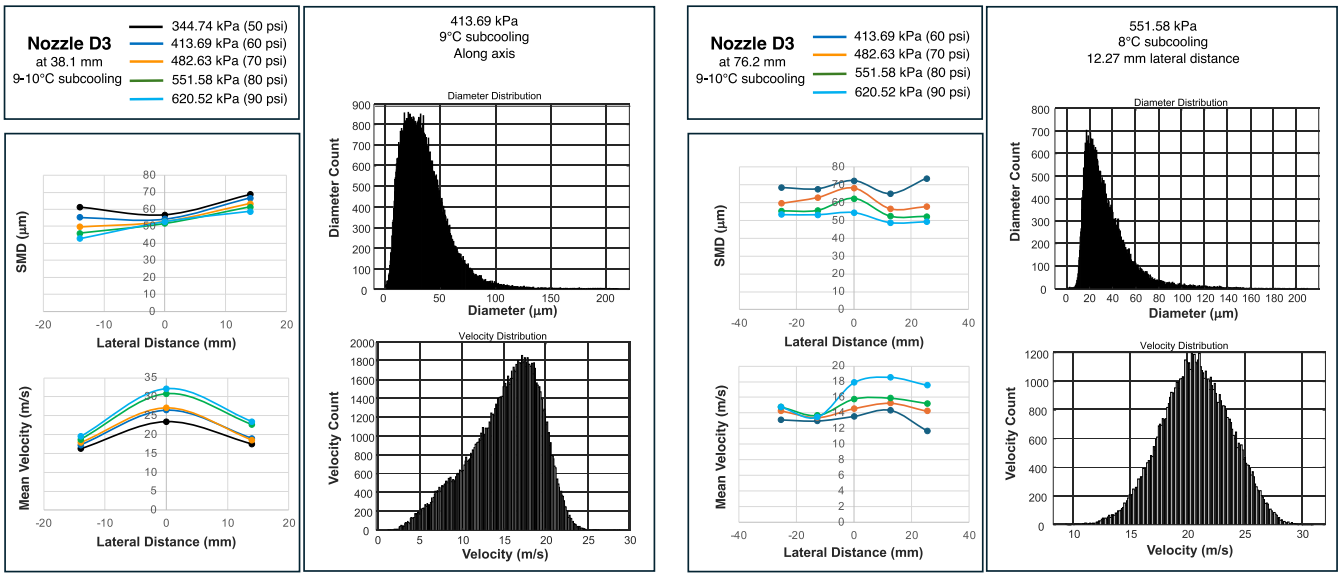

Fig. 10a. PDPA measurements for nozzle D3 at axial distances of 38.1 and 76.2 mm.

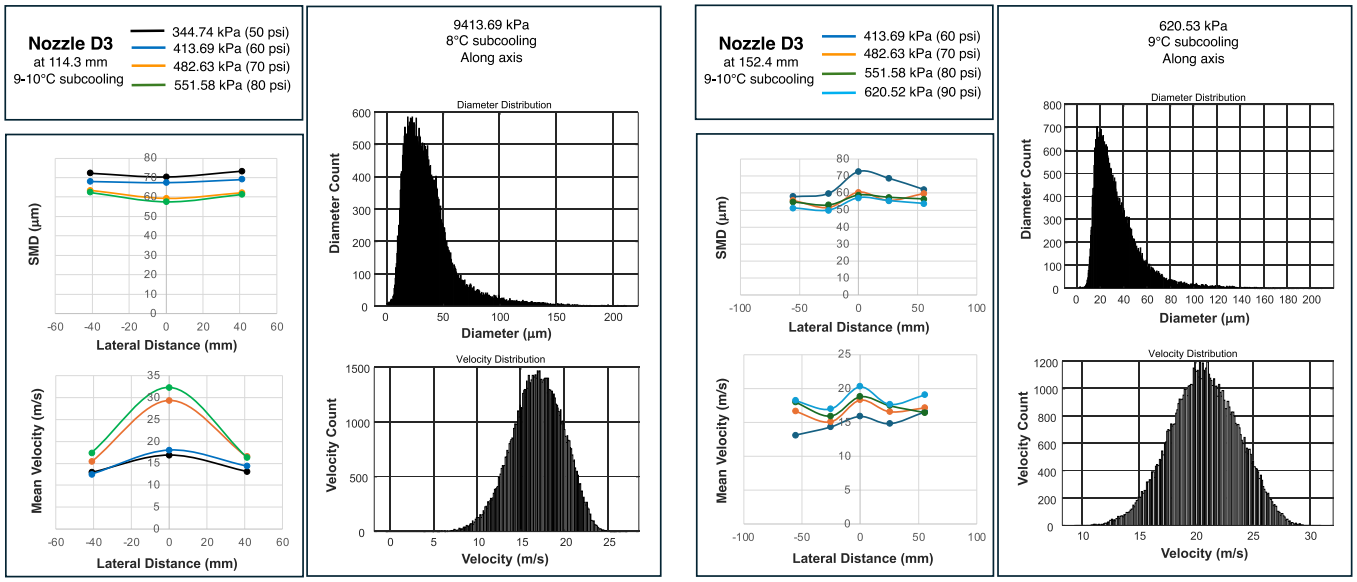

Fig. 10b. PDPA measurements for nozzle D3 at axial distances of 114.3 and 152.4 mm.

collected for liquid nitrogen (LN_2) sprays. The primary metric used to evaluate the predictive accuracy of these correlations is the Mean Absolute Error (MAE), which quantifies the average magnitude of error between predicted and measured values, regardless of direction. The MAE is defined as:

$$MAE = \frac{1}{N}\sum_{i=1}^{N}\left|\frac{Pred_i - Meas_i}{\text{Meas}_i}\right| \times 100 \quad (1)$$

where $Pred_i$ and $Meas_i$ are the predicted and measured values, respectively, and N the total number of data points.

There have been several previous efforts to develop empirical correlations for spray parameters, aimed at enabling predictive design tools for specific applications. However, most of these correlations were derived using fluids such as water, dielectric coolants, or other non-cryogenic liquids. Cryogenic fluids like liquid nitrogen (LN_2), by contrast, present far greater challenges due to their much lower saturation temperatures and distinctly different thermophysical properties—such as lower liquid viscosity, reduced surface tension, and lower latent heat of vaporization. Additionally, cryogenic sprays are highly susceptible to rapid evaporation and flashing when exposed to ambient conditions, which further complicates measurement and prediction. These fundamental differences underscore the need for fluid-specific correlations tailored to the unique behavior of cryogenic sprays.

To aid in developing new LN_2 spray correlations, the present experimental data are compared with predictions from nine previously published correlations for Sauter Mean Diameter (SMD) and Mass Median Diameter (d_{50}). Table 2 summarizes each correlation along with its corresponding MAE when applied to the LN_2 dataset.

The Sauter Mean Diameter (SMD) is the most commonly used statistical metric for characterizing spray droplet size. It represents the diameter of a droplet that has the same volume-to-surface-area ratio as the average droplet in the spray, making it particularly relevant in heat and mass transfer applications where surface area is critical. In contrast, the Mass Median Diameter (MMD or d_{50}) refers to the droplet diameter at which half of the total mass of the spray is composed of smaller

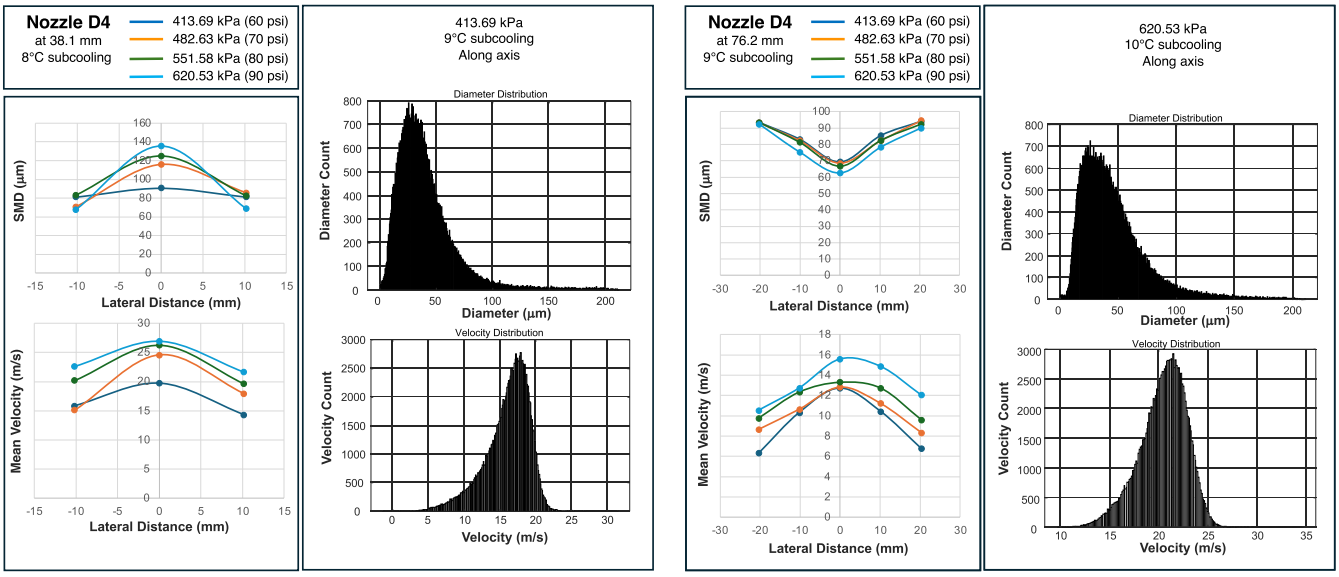

Fig. 11a. PDPA measurements for nozzle D4 at axial distances of 38.1 and 76.2 mm.

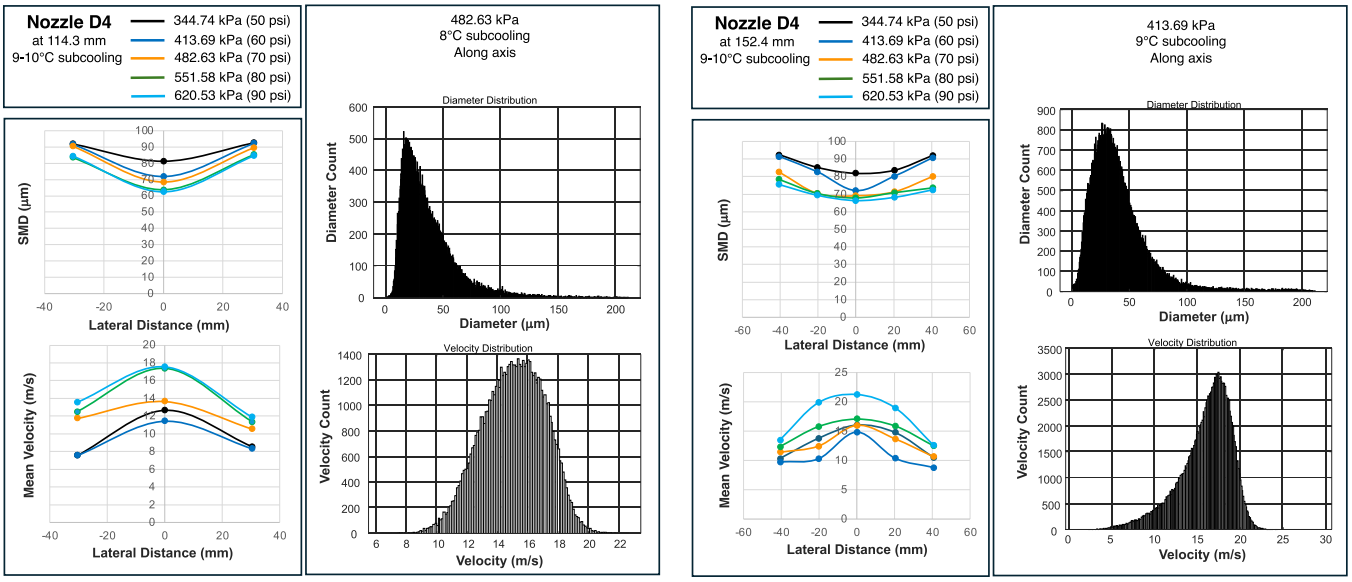

Fig. 11b. PDPA measurements for nozzle D4 at axial distances of 114.3 and 152.4 mm.

droplets and half is composed of larger ones. SMD is defined as

$$SMD = d_{32} = \frac{\sum n_i d_i^3}{\sum n_i d_i^2} \tag{2}$$

It is worth noting that some of the evaluated correlations are dimensionless, while others are based on dimensional formulations. In the two-phase flow and heat transfer literature, dimensionless correlations are generally preferred due to their reliance on physical similarity parameters and their broader applicability across different fluids. For instance, reference [16] demonstrated a dimensionless correlation capable of accurately capturing spray behavior for both water and FC-72—fluids with markedly different thermophysical properties. However, applying existing correlations to liquid nitrogen (LN_2) introduces additional complexity, given its significantly lower saturation temperature and highly distinct thermophysical properties relative to more commonly studied fluids. The uniqueness of LN_2 is further highlighted by the large Mean Absolute Errors (MAEs) associated with six of the nine previously published correlations—both dimensional and dimensionless—with some predictions deviating by more than 1000 %.

In this study, new correlations are developed based on the present LN_2 data for the two most commonly used droplet diameters: d_{32} and d_{10}. The latter is the Arithmetic Mean Diameter (MD), which is defined as

$$d_{10} = \frac{\sum n_i d_i}{\sum n_i} \tag{3}$$

The formulation of the two new correlations for LN_2 is based on two key dimensionless groups: the Reynolds number for the liquid phase (Re_f) and the Weber number for the liquid phase (We_f). Re_f represents the ratio of inertial forces to viscous forces within the liquid flow, while We_f quantifies the ratio of inertial forces to surface tension forces. The new correlations are given as follows:

$$\frac{d_{32}}{d_0} = 1.357 We_f^{-0.101} Re_f^{-0.15} \tag{4}$$

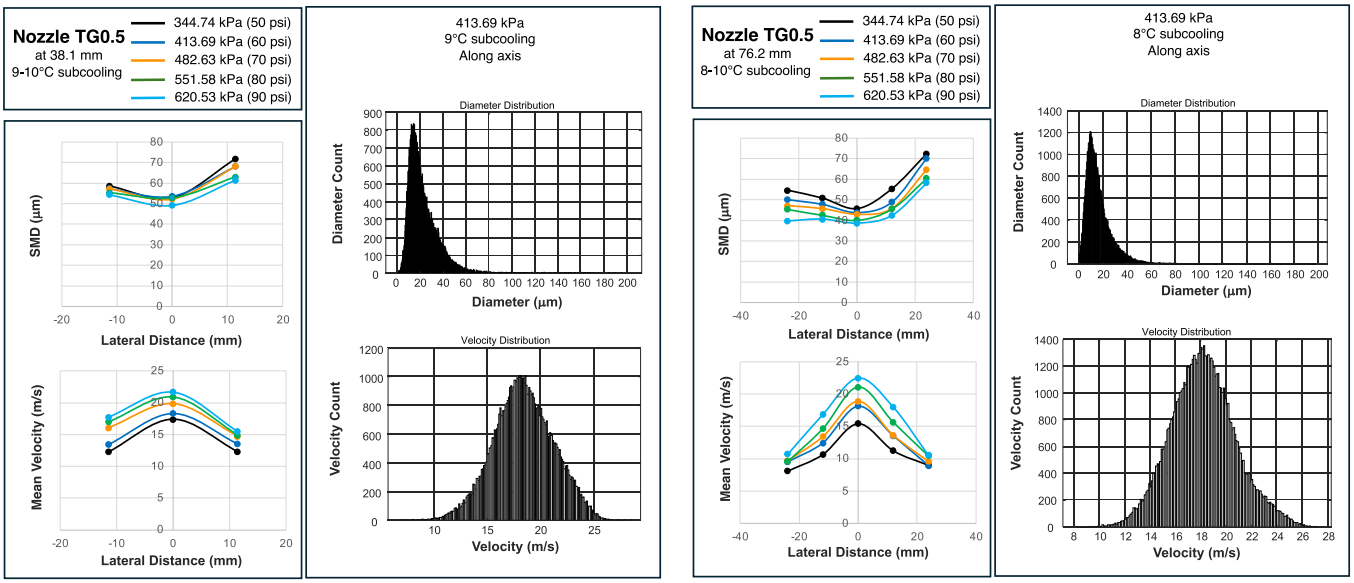

Fig. 12a. PDPA measurements for nozzle TG0.5 at axial distances of 38.1 and 76.2 mm.

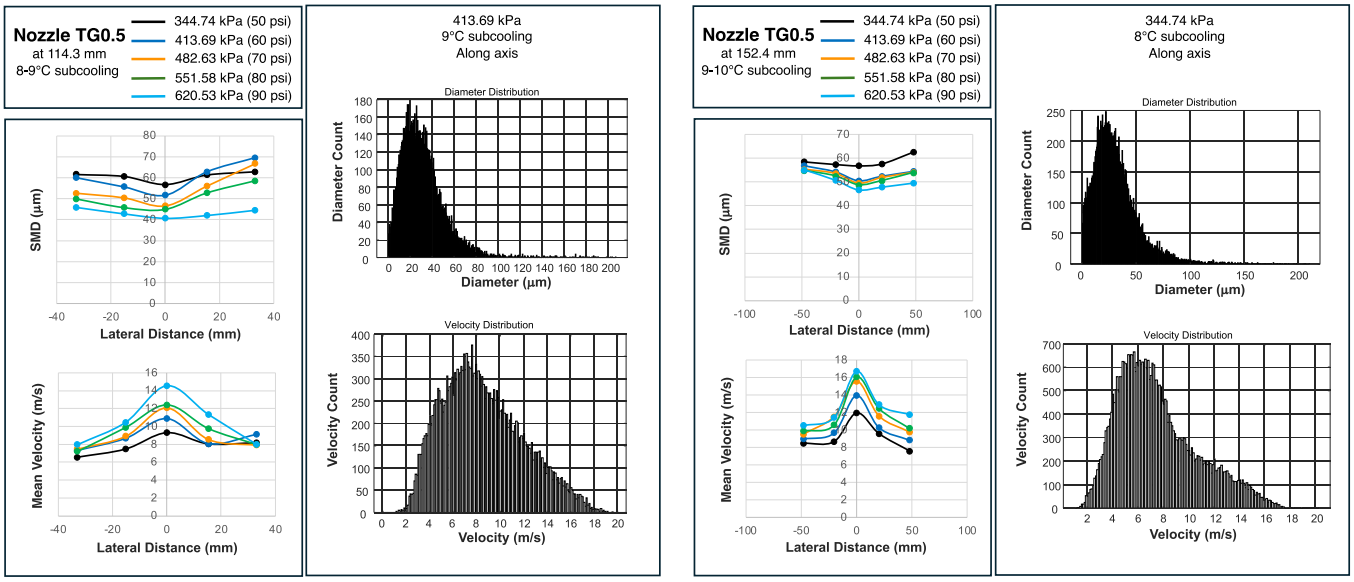

Fig. 12b. PDPA measurements for nozzle TG0.5 at axial distances of 114.3 and 152.4 mm.

$$\frac{d_{10}}{d_0} = 35.84 We_f^{-0.293} Re_f^{-0.293} \tag{5}$$

Figs. 14(a) and 14(b) present comparisons between the predictions of the newly developed correlations and the experimental LN_2 data for d_{32} and d_{10}, respectively. The accuracy of the correlations is reflected in the relatively low MAEs, which are 16.19 % for d_{32} and 17.63 % for d_{10}, indicating good agreement with the measured data.

In addition to the droplet size correlations, a separate correlation is formulated for the Mean Droplet Velocity (u_f), also expressed as a function of Re_f and We_f.

$$\frac{u_f}{\sqrt{\frac{2\Delta P}{\rho_f}}} = 8.817 \left(\frac{We_f}{Re_f}\right)^{0.495} \tag{6}$$

The dimensionless velocity expression presented in Eq. (6) is identical to that proposed in [16]. Notice that We_f/Re_f can also be expressed as $(\mu U_f)/\sigma$, ratio of viscous force to surface tension force. Fig. 15 illustrates the performance of the new Mean Droplet Velocity correlation against the experimental LN_2 data. The correlation demonstrates good predictive capability, as evidenced by a MAE of 23.61 %.

The valid ranges for the present correlations are between 43,111 – 533,861 for Re_f and 55,126 – 442,980 for We_f. Two limitations of these correlations are applicability to LN_2 and to swirl type nozzles. While these correlations might be applicable to other cryogens and nozzle types, ascertaining such applicability will require additional experimental work.

3.3. Cone angle

The spray cone angles for the different nozzles were measured from video images as outlined in Section 2.3. This procedure was repeated across a range of injection pressures to identify any observable trends. The results, presented in Fig. 16 and Table 3, indicate that the cone angle values remain relatively consistent, varying within 10 % to 15 % of the mean value for each nozzle. These findings are consistent with the

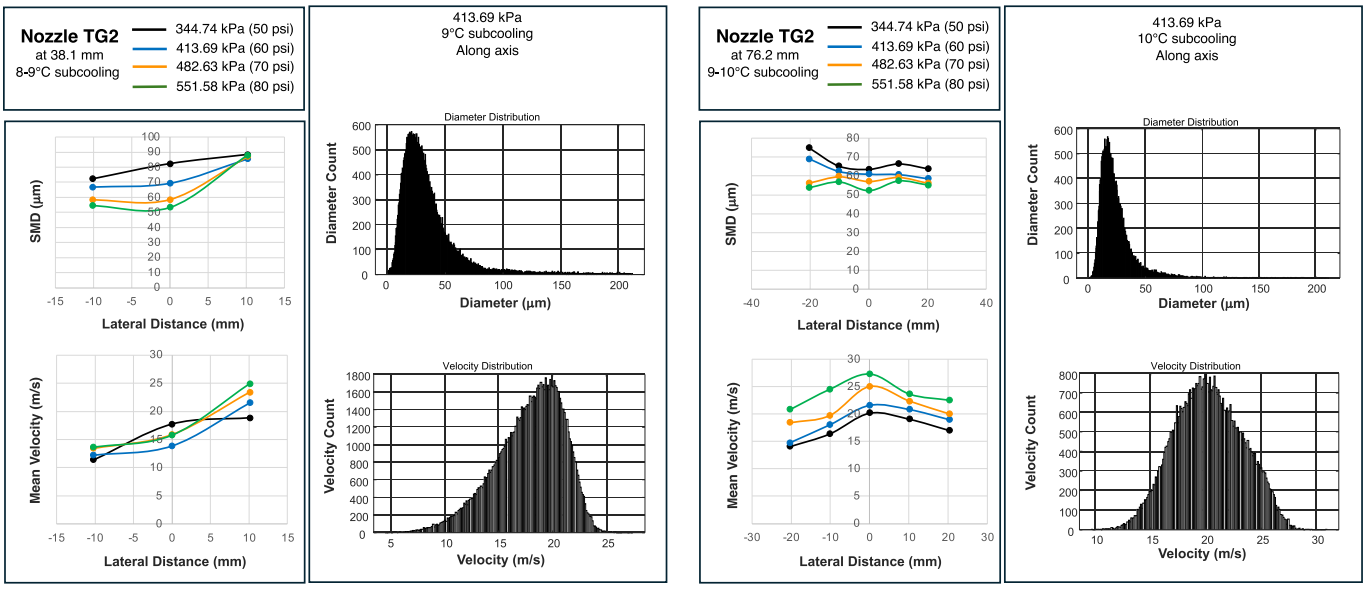

Fig. 13a. PDPA measurements for nozzle TG2 at axial distances of 38.1 and 76.2 mm.

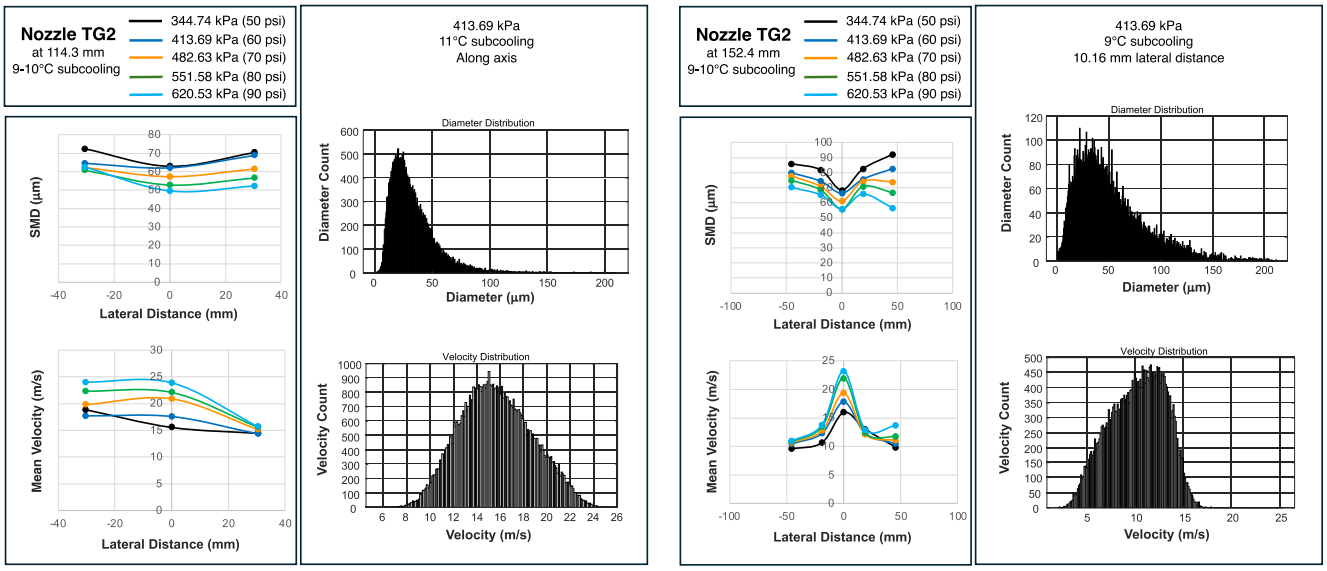

Fig. 13b. PDPA measurements for nozzle TG2 at axial distances of 114.3 and 152.4 mm.

observations reported by Xue et al. [19], who also noted stable cone angles across different injection pressures. When compared to the average cone angles provided by the nozzle manufacturer (Spraying Systems) for water sprays, the measured cone angles for LN_2 are smaller. This discrepancy can be primarily attributed to the distinct thermophysical properties of LN_2. Additionally, heat transfer from the warmer ambient environment to the LN_2 droplets may lead to evaporation at the spray's outer periphery—where droplet density is lowest—thereby reducing the overall cone angle.

3.4. Droplet breakup regimes

In addition to developing predictive tools for droplet diameter and velocity, it is essential to investigate the initial breakup patterns and droplet formation mechanisms in LN_2 sprays. The breakup of a liquid jet emerging from an orifice is a complex process governed by a combination of inertial, surface tension, viscous, and aerodynamic forces. Several studies have explored the instability mechanisms that govern jet disintegration. A widely adopted classification, proposed by Ohnesorge [28], categorizes jet breakup regimes based on the Ohnesorge number (*Oh*), which represents the ratio of viscous forces to the square root of the product of inertial and surface tension forces.

Further refinements to Ohnesorge's [39] breakup regime classification have been proposed by researchers such as Castleman [40], Miesse [41], and Reitz [42], who incorporated additional breakup mechanisms and revised the boundaries between regimes. Castleman [40] highlighted the importance of the relative motion between the outer layer of the jet and the surrounding air, which induces surface instabilities and the formation of ligaments—elongated fluid structures that eventually fragment into smaller droplets. Building on these insights, Miesse [41] conducted experimental investigations that led to a shift in the boundary between the Rayleigh and Wavy regimes. His findings prompted the development of an updated empirical relation to more accurately predict the onset of jet breakup under varying flow conditions. Reitz [42] further expanded the classification of jet breakup mechanisms by introducing a four-regime framework, as opposed to the earlier three-

Table 2
Predictions of prior correlations for SMD and MMD against present LN_2 data, and corresponding MAE.

Author(s) [ref] year	Correlation	Fluid(s)	Notes	MAE
Merrington & Richardson [31] 1947	$d_{32} = 500\frac{d_0^{1.2}\nu_f^{0.2}}{U_f}$	Water		200 %
Panasenkov [32] 1951	$\frac{d_{50}}{d_0} = 6\mathrm{Re}_f^{-0.15}$	Water		≫ 100 %
Harmon [33] 1955	$d_{32} = 3,330 d_0^{0.3}\mu_f^{0.07}\rho_f^{-0.048}\sigma^{-0.15}u_f^{-0.15}\mu_a^{0.78}\rho_a^{-0.052}$	Water		≫ 100 %
Tanasawa & Toyoda [34] 1955	$\frac{d_{32}}{d_0} = 47U_f^{-1}\left(\frac{\sigma}{\rho_G}\right)^{0.25}\left[1+331\frac{\mu_f}{(\rho_f\sigma d_0)^{05}}\right]$	Water, Fuel		≫ 100 %
Hiroyasu & Katota [35] 1974	$d_{32} = 2330\rho_a^{0.121}Q^{0.131}\Delta P^{-0.135}$	Water		≫ 100 %
Elkotb [36] 1974	$d_{32} = 3.08\nu_f^{0.385}\sigma^{0.737}\rho_f^{0.737}\rho_a^{0.06}\Delta P^{-0.54}$	Fuel		≫100 %
Estes & Mudawar [16] 1995	$\frac{d_{32}}{d_0} = 3.07\left[\frac{\rho_f^{1/2}\Delta P d_0^{1/2}}{\sigma^{1/2}\mu_f}\right]^{-0.290}$	FC-72, Water	Unijet nozzles: d_0 = 0.61–0.9 mm	225 %
Cleary et al. [37] 2007	$\frac{d_{32}}{d_0} = 64.73\left(\frac{L}{d_0}\right)^{0.114}Re_f - 0.014\,\mathrm{We}_f^{-0.533}$	Water	Flashing jets d_0 = 0.75–1.0 mm	90.42 %
Lefebvre & McDonell [38] 2017	$d_{32} = 2.25\sigma^{2.25}\mu_f^{0.25}\dot{m}^{0.25}\Delta P^{-0.25}\rho_a^{-0.25}$	Water	Pressure swirl	≫ 100 %

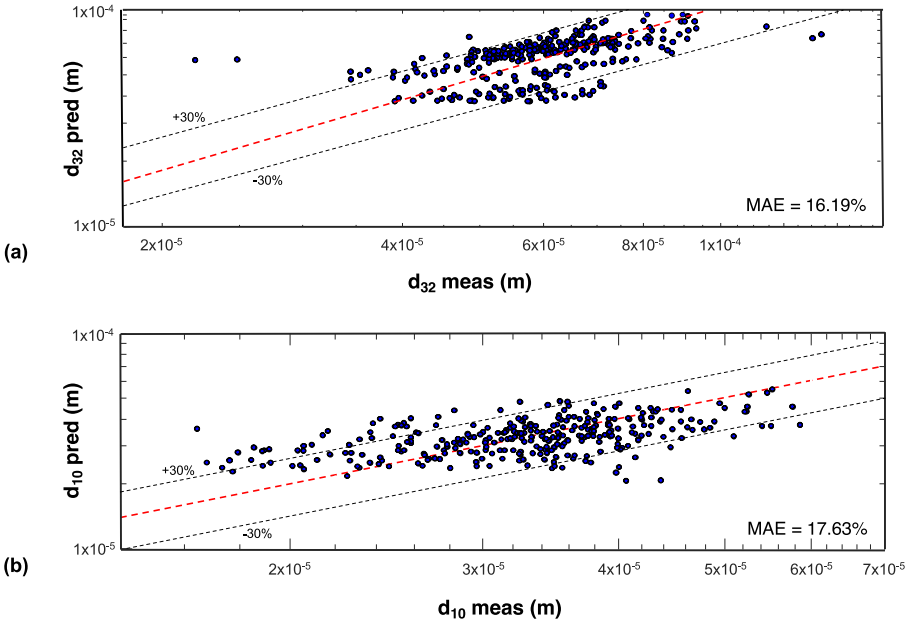

Fig. 14. Comparison of predictions of new correlations with LN_2 experimental data for (a) d_{32} and (b) d_{10}.

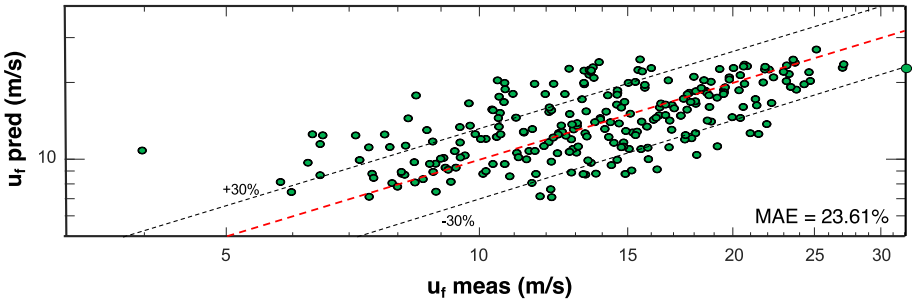

Fig. 15. Comparison of predictions of new correlations with LN_2 experimental data for Mean Droplet Velocity.

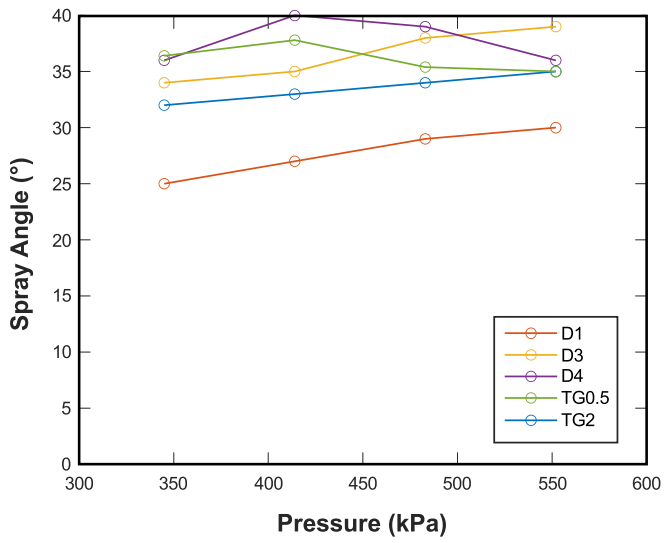

Fig. 16. Variation of cone angle with injection pressure for LN_2 for the different nozzles.

Table 3
Cone angle variance with injection pressure for LN_2 and comparison with average cone angle for water sprays provided by the nozzle manufacturer.

	Injection Pressure (kPa)				
	344.74	413.69	483.63	551.58	
Nozzle	Average Cone Angle for LN_2 [degrees]				Average Cone Angle for water [degrees]
D1	25	27	29	30	45
D3	34	35	38	39	53
D4	36	40	39	36	55.8
TG0.5	36	37	35	35	56
TG2	32	33	34	35	48

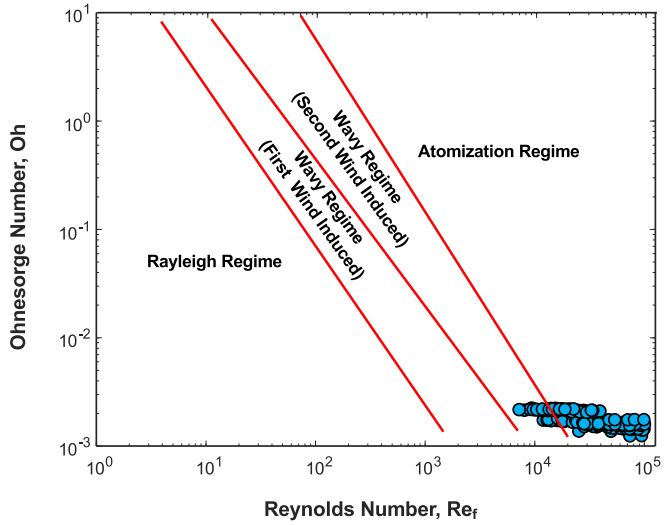

Fig. 17. Current LN_2 data points superimposed on droplet breakup regimes map from [27].

regime models.

Lefebvre and McDonell [38] provided a graphical representation of the various jet breakup regimes using a plot of *Oh* versus Re_f. As shown in Fig. 17, the Rayleigh, Wavy, and Atomization Regimes correspond to low, intermediate, and high Re_f values, respectively. Superimposed on this plot are the data points from the present LN_2 experiments. These clearly fall within the Atomization Regime, indicating that droplet breakup in this study is primarily governed by high-velocity, aerodynamic-driven disintegration typical of atomization processes.

4. CONCLUSIONS

This study presents comprehensive measurements of droplet diameter and velocity for liquid nitrogen (LN_2) sprays discharged into ambient air. Using a high-resolution Phase Doppler Particle Analyzer (PDPA), the research captured both mean values and statistical distributions of droplet size and velocity. Five full-cone spray nozzles were tested across a range of injection pressures. From these experiments, new correlations were developed for Sauter Mean Diameter (d_{32}), Arithmetic Mean Diameter (d_{10}), and Mean Droplet Velocity (u_f), tailored specifically for LN_2. These correlations offer predictive capabilities critical for the design of cryogenic spray systems, including applications in future space technologies. Key findings from the study include:

1. Injection pressure significantly influences spray characteristics. An increase in injection pressure consistently led to a decrease in d_{32} and an increase in u_f across all tested nozzles.
2. Axial and lateral variations in d_{32} and u_f exhibited notable inconsistencies, attributed to differences in near-nozzle breakup dynamics, levels of subcooling, and the extent of ambient vaporization.
3. The statistical distribution of u_f follows a Gaussian profile, whereas the distribution of d_{32} is skewed toward smaller droplet sizes.
4. Existing d_{32} correlations—primarily developed for water—demonstrate poor predictive accuracy when applied to the current LN_2 spray data, highlighting the need for fluid-specific correlations.
5. New dimensionless correlations for droplet diameters, based on Reynolds and Weber numbers, were developed specifically for LN_2. These correlations demonstrated strong predictive performance, with mean absolute errors (MAEs) of 16.19 % for d_{32} and 17.63 % for d_{10}.
6. A new dimensionless correlation for u_f was formulated as a function of injection pressure, Reynolds number, and Weber number. This correlation showed good agreement with the LN_2 experimental data, achieving a MAE of 23.61 %.
7. Spray cone angle is largely insensitive to injection pressure, but consistently smaller than the manufacturer's specified angle for water sprays. This discrepancy is attributed to significant differences in thermophysical properties—such as liquid viscosity, surface tension, and latent heat of vaporization—between LN_2 and water. Additionally, heat transfer from the warmer ambient environment to the LN_2 droplets induces evaporation at the spray's outer edges, where droplet density is lowest, further contributing to the reduced cone angle.
8. Droplet breakup in the LN_2 sprays predominantly falls within the Atomization Regime, indicating the dominance of strong inertial and aerodynamic forces in the breakup process.
9. Future work can benefit from high-resolution CT (or equivalent method) to quantify internal features of spray nozzles and preclude effects of machining imperfections.

CRediT authorship contribution statement

Nishad Damle: Writing – review & editing, Writing – original draft, Visualization, Validation, Software, Methodology, Investigation, Formal analysis, Data curation, Conceptualization. **Issam Mudawar:** Writing – review & editing, Writing – original draft, Validation, Supervision, Resources, Project administration, Methodology, Investigation, Funding acquisition, Formal analysis, Conceptualization. **Jason Hartwig:** Writing – review & editing, Writing – original draft, Validation, Supervision, Resources, Project administration, Methodology, Investigation, Funding acquisition, Formal analysis, Conceptualization.

Declaration of competing interest

The authors declare that they have no known competing financial interests or personal relationships that could have appeared to influence the work reported in this paper.

Acknowledgement

The authors would like to thank Dr. Wing Lai for his expertise and support in PDPA for this study. The authors are appreciative of the support of the National Aeronautics and Space Administration (NASA) under grant no. 80NSSC23K0228.

Data availability

The data that has been used is confidential.

References

[1] A. LeClair, M. Baldwin, A. Majumdar, J. Hartwig, V. Ganesan, I. Mudawar, Modeling of cryogenic heated-tube flow boiling experiments of hydrogen and helium with the Generalized Fluid System Simulation Program, Cryogens 143 (2024) 103926.
[2] J.W. Hartwig, A. Asensio, S.R. Darr, Assessment of existing two phase heat transfer coefficient and critical heat flux on cryogenic flow boiling quenching experiments, Int. J. Heat Mass Transf. 93 (2016) (2016) 441–463.
[3] T.J. LaClair, I. Mudawar, Thermal transients in a capillary evaporator prior to the initiation of boiling, Int. J. Heat Mass Transf. 43 (2000) 3937–3952.
[4] G. Liang, I. Mudawar, Pool boiling critical heat flux (CHF) – part 2: assessment of models and correlations, Int. J. Heat Mass Transf. 117 (2018) 1368–1383.
[5] I. Mudawar, R.A. Houpt, Mass and momentum transport in smooth falling liquid films laminarized at relatively high Reynolds numbers, Int. J. Heat Mass Transf. 36 (1993) 3437–3448.
[6] C.R. Kharangate, H. Lee, I. Mudawar, Computational modeling of turbulent evaporating falling films, Int. J. Heat Mass Transf. 81 (2015) 52–62.
[7] T.C. Willingham, I. Mudawar, Channel height effects on forced-convection boiling and critical heat flux from a linear array of discrete heat sources, Int. J. Heat Mass Transf. 35 (1992) 1865–1880.
[8] C.O. Gersey, I. Mudawar, Effects of heater length and orientation on the trigger mechanism for near-saturated flow boiling critical heat flux - II, Critical heat flux model, Int J Heat Mass Transf 38 (1995) 643–654.
[9] H. Lee, I. Park, I. Mudawar, M.M. Hasan, Micro-channel evaporator for space applications-1, Experimental pressure drop and heat transfer results for different orientations in earth gravity, Int J Heat Mass Transf 77 (2014) 1213–1230.
[10] M.T. Meyer, I. Mudawar, C.E. Boyack, C.A. Hale, Single and two-phase cooling with an array of rectangular jets, Int. J. Heat Mass Transf. 49 (2006) 17–29.
[11] I. Mudawar, T.A. Deiters, A universal approach to predicting temperature response of metallic parts to spray quenching, Int. J. Heat Mass Transf. 37 (1994) 347–362.
[12] M.K. Sung, I. Mudawar, Single-phase and two-phase hybrid cooling scheme for high-heat-flux thermal management of defense electronics, J. Electron. Packag. 131 (2009) 021013.
[13] I. Mudawar, Recent advances in high-flux, two-phase thermal management, J Thermal Sci Eng Appl 5 (2013) 021012.
[14] G. Liang, I. Mudawar, Review of spray cooling – part 1: single-phase and nucleate boiling regimes, and critical heat flux, Int. J. Heat Mass Transf. 115 (2017) 1174–1205.
[15] G. Linag, I. Mudawar, Review of spray cooling – part 2: high-temperature boiling regimes and quenching applications, Int. J. Heat Mass Transf. 115 (2017) 1206–1222.
[16] A.E. Estes, I. Mudawar, Correlations of Sauter Mean Diameter and critical heat flux for spray cooling of small surfaces, Int. J. Heat Mass Transf. 38 (1995) 2985–2996.
[17] W.S. Valentine, I. Mudawar, Determination of the local quench curve for spray-cooled metallic surfaces, J. Heat. Treat. 7 (1989) 107–121.
[18] X. Liu, R. Xue, Y. Ruan, L. Chen, X. Zhang, Y. Hou, Effects of injection pressure difference on droplet size distribution and spray cone angle in spray cooling of liquid nitrogen, Cryogenics 83 (2017) 57–63.
[19] R. Xue, Y. Ruan, X. Liu, L. Chen, X. Zhang, Y. Hou, S. Chen, Experimental study of liquid nitrogen spray characteristics in atmospheric environment, Appl. Therm. Eng. 142 (2018) 717–722.
[20] A. Rees, L. Araneo, H. Salzmann, G. Lamanna, J. Sender, M. Oschwald, Droplet velocity and diameter distributions in flash boiling liquid nitrogen jets by means of phase Doppler diagnostics, Exp. Fluids 61 (2020) 1–18.
[21] N. Fdida, Y. Mauriot, L. Vingert, A. Ristori, M. Théron, Characterizing primary atomization of cryogenic LOX/nitrogen and LOX/helium sprays by visualizations coupled to Phase Doppler Interferometry, Acta Astronaut 164 (1019) 458–465.
[22] R.D. Ingebo, Effect of vaporization on cryogenic spray dropsize measurement, NASA Tech. Memo. 105909 (1992).
[23] J. Wang, C. Xu, G. Zhou, Y. Zhang, Spray structure and characteristics of a pressure-swirl nozzle dust suppression nozzle using a Phase Doppler Analyzer, Processes 8 (2020) 1127.
[24] S.K. Soni, P.S. Kolhe, Liquid jet breakup and spray formation with annular swirl air, Int. J. Multiph. Flow 134 (2021) 103474.
[25] S. Patil, S. Sahu, Air swirl effect on spray characteristics and droplet dispersion in a twin-jet crossflow airblast injector, Phys. Fluids 33 (2021) 073314.
[26] X. Li, S. Yang, Z. Sun, S. Wang, S. Qiu, S.L.S. Hung, M. Xu, A review on the recent advances of flash boiling atomization and combustion applications, Prog. Energy Combust. Sci. 100 (2024) 101119.
[27] M.S. Akram, Q. Cheng, O. Kaario, M. Larmi, Superheated fuel sprays: A comparative study of flash boiling ammonia fuel sprays with methanol, ethanol, and gasoline for multi-hole fuel injection, Case Stud. Therm. Eng. 61 (2024) 105110.
[28] R. Payri, P. Marti-Aldaravi, R. Abboud, A. Bautista, Numerical analysis of GDI flash boiling sprays using different fuels, Energies 14 (2021) 5925.
[29] C. An, L. Liu, H. Luo, B. Zhou, Y. Liu, X. Li, K. Nishida, Threshold sensitivity study on spray–spray impingement under flexible injection strategy for fuel/air mixture evaluation, Phys. Fluids 37 (2025) 065124.
[30] C. Zhai, J. Zhang, K. Li, P. Dong, Y. Jin, F. Chang, H. Luo, Comparative analysis and normalization of single-hole vs. multi-hole spray characteristics: 1st report on spray characteristic comparison, Green Energy Resour. 3 (2025) 100120.
[31] A.C. Merrington, E.G. Richardson, The break-up of liquid jets, Proc. Phys. Soc. London 59 (1947) 1–13.
[32] N.J. Panasenkov, Effect of the turbulence of a liquid jet on its atomization Zh Tekh Fiz 21 (1951) 160.
[33] D.B. Harmon, Drop sizes from low-speed jets, J. Franklin Inst. 259 (1955) 519–522.
[34] Y. Tanasawa, S. Toyoda, On the atomization of a liquid jet issuing from a cylindrical nozzle, Technical Reports of Tohoku Univ, Japan 19 (2) (1955) 135–140.
[35] H. Hiroyasu, T. Katota, Fuel droplet size distribution in a diesel combustion chamber, SAE Trans, Paper 740715, 1974.
[36] M.M. Elkotb, Fuel atomization for spray modeling, Prog Energ Combust Sci 8 (1982) 61–91.
[37] V. Cleary, P. Bowen, H. Witlox, Flashing liquid jets and two-phase droplet dispersion I, Experiments for derivation of droplet atomization correlations, J Hazard Mater 142 (2007) 786–796.
[38] H. Lefebvre, V.G. McDonell, Atomization and sprays, 2nd ed., CRC Press, 2017.
[39] W. Ohnesorge, The formation of drops by nozzles and the breakup of liquid jets, Z. Angew. Math. Mech. 16 (1936) 355–358.
[40] R.A. Castelman, The mechanism of the atomization of liquids, J. Res. Natl. Bur. Stand. 6 (1931) 369–376.
[41] C.C. Miesse, Correlation of experimental data on the disintegration of liquid jets, Ind. Eng. Chem. 47 (1955) 1690–1701.
[42] R.D. Reitz, Atomization and other breakup regimes of a liquid jet, Princeton University, Princeton, NJ, 1978. Ph.D. thesis.